ACADEMIC PRESS

Available online at www.sciencedirect.com
SCIENCE DIRECT®

Journal of Colloid and Interface Science 259 (2003) 62–80

JOURNAL OF Colloid and Interface Science

www.elsevier.com/locate/jcis

Investigation of a colloidal damper

C.V. Suciu,[a,*] T. Iwatsubo,[b] and S. Deki [c]

[a] *Graduate School of Science and Technology, Kobe University, 1-1 Rokkodai, Nada, Kobe, Hyogo 657-8501, Japan*
[b] *Mechanical Engineering Department, Faculty of Engineering, Kobe University, 1-1 Rokkodai, Nada, Kobe, Hyogo 657-8501, Japan*
[c] *Department of Chemical Science and Engineering, Faculty of Engineering, Kobe University, 1-1 Rokkodai, Nada, Kobe, Hyogo 657-8501, Japan*

Received 4 February 2002; accepted 16 October 2002

Abstract

A novel application of nanotechnology in the field of mechanical engineering, called colloidal damper (CD), is investigated. This device is complementary to the hydraulic damper (HD), having a cylinder-piston construction. Particularly for CD, the hydraulic oil is replaced by a colloidal suspension, which consists of a mesoporous matrix and a lyophobic fluid. In this work, the porous matrix is from silica gel modified by linear chains of *n*-alkylchlorosilanes and water is considered as an associated working fluid. A design solution from a practical point of view of the CD test rig and the measuring technique of the hysteresis are described. A brief review of the water physical properties relative to the CD concept is presented. Influence of the bonding density, length of the grafted molecule, pore diameter, and particle diameter on the CD hysteresis is investigated for distinctive types and mixtures of silica gels. Temperature variation during functioning is recorded and the CD cycle is interpreted from a thermodynamic standpoint. Variation of the CD dissipated energy and efficiency with pressure, water quantity, and relaxation time is illustrated. Experimental results are justified by the analysis of the water flow into the porous matrix, CD thermodynamics, and the mechanism of the energy dissipation. Our findings agree with the previously published data.
© 2003 Elsevier Science (USA). All rights reserved.

Keywords: Colloid; Damping; Nanotechnology; Hydrophobic porous silica gel; Ink-bottle theory; Contact angle hysteresis; Creeping flow; Slip

1. Introduction

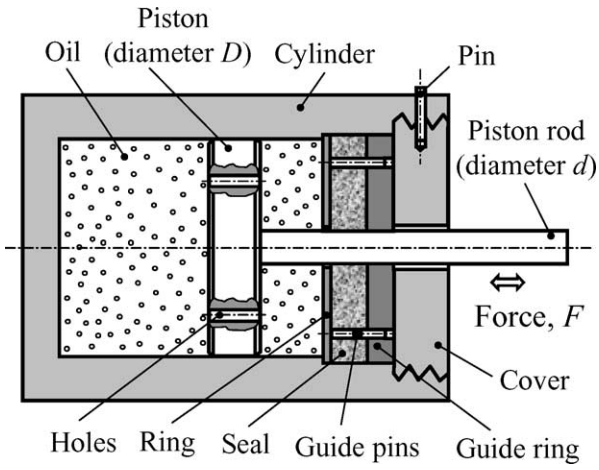
Ability of fluids, flowing in narrow interstices, to dissipate the energy of shock and vibration is well known [1–4], the specialized machine element being called viscous damper. The fluid flow can be Couette (Lanchester's absorber) or/and Poiseuille (hydro-pneumatic dampers, squeeze film dampers, etc.). The colloidal damper (CD), proposed by Eroshenko [5–7], is a device complementary to the hydraulic damper (HD), having a cylinder-piston construction (Fig. 1). The solid porous matrix and its associated lyophobic fluid produce a colloidal suspension, which suggests the damper denomination. The porous matrix can be from [5,6,8,9] silica gel, aerogel, ceramics, glass, zeolites, carbon (graphite, charcoal, fullerenes), aluminum oxide, etc. The associated lyophobic fluid (the surface of the matrix is not wetted by the fluid) can be [6] water, aqueous solutions (e.g., water and antifreeze agent), mercury, melted metals (e.g., lead), melted alloys (e.g., wood alloy, eutectics), melted flux, melted salts, etc. Convenient from the ecological and economical point of view is the combination silica gel–water [9–12]. In the present work, only this type of colloidal suspension is considered. Silica gel matrix (Fig. 2) consists of porous microparticles of radius b. The mesopores, of variable radius a, occur as intersected tubes, which follow complex directions. The whole (inner and outer) surface of the particles is hydrophobized with *n*-alkylchlorosilanes [13,14]. At compression (Fig. 1b), water is forced to penetrate the porous matrix (Fig. 2). External pressure p works against the Laplace capillary pressure $(-2\sigma\cos\theta/a)$ and the pressure of the gas trapped into the porous matrix p_g, which tend to push out the water

$$p = -2\sigma\cos\theta/a + p_g. \tag{1}$$

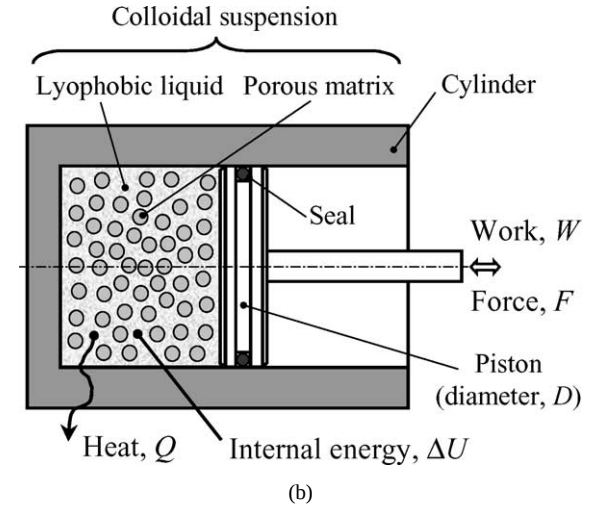
Later, a detailed discussion concerning Eq. (1) will be made. By analogy with the mercury porosimetry [15–18], this mechanism was called water porosimetry [14,19,20]. The CD concept is based on the observation that the compression and relaxation paths in the p–V (pressure–volume) or F–s (force–stroke) coordinates (Fig. 11) are not superposed and

* Corresponding author.
E-mail addresses: 989d847n@yku.kobe-u.ac.jp (C.V. Suciu), iwatsubo@mech.kobe-u.ac.jp (T. Iwatsubo), deki@kobe-u.ac.jp (S. Deki).

0021-9797/03/$ – see front matter © 2003 Elsevier Science (USA). All rights reserved.
doi:10.1016/S0021-9797(02)00076-0



(a)



(b)

Fig. 1. Schematic view of HD (a) and CD (b).

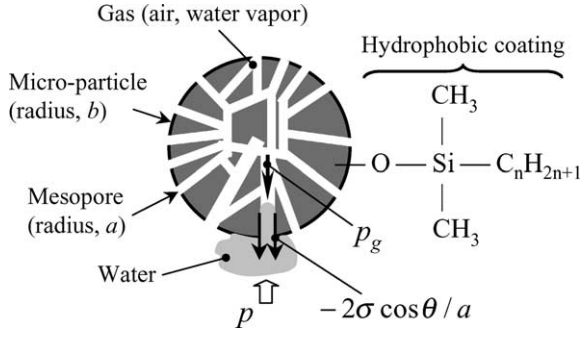


Fig. 2. Water penetration into a hydrophobic matrix of mesoporous silica gel.

a hysteresis occurs [14,16,19]. The dissipated energy equals the area of the hysteresis [9,21,22]. Thus, the same phenomenon, which lies at the basis of the water porosimetry, is employed here to dissipate the energy of shock and/or vibration. Figures 1 and 2 illustrate that both HD and CD dissipate the mechanical energy by forcing the working fluid to pass through narrow orifices [1,22]. The difference between them is the size of the orifices, which is on order of millimeters for HD and nanometers for CD. However, compared with HD, CD behaves unusually: it is able to absorb a large amount of mechanical energy, without heating [5,6,22]; the CD force is not depending on the piston velocity [7]; the CD frequency range (0–30 Hz) is 5 times higher [7]; and the CD efficiency is 2 times higher [5,6,9,22]. Due to these important advantages, CD can be employed for vehicle suspensions, seismic dampers, buffers, engines supports, various antivibration protections, etc. CD can be regarded as a novel application of nanotechnology in the field of mechanical engineering. Its investigation represents a fundamental research in the controversial field of fluid properties when present in mesopores, requiring interdisciplinary approach: interface and colloid science, thermodynamics, fluid dynamics, and vibration and machine dynamics. Experimental investigations of the water intrusion and extrusion (water porosimetry technique) from a porous silica matrix, preliminarily subjected to chemical modification, are presented in Refs. [14,19,20]. It was proved that when the length of the grafted alkyl chain increases, the pressures of intrusion and extrusion of water from the pore space increase, the advancing and receding contact angles increase, and the mean radius of the pores decreases. It was suggested that “friction” at the wetting line might be the origin of the hysteresis observed [19]. A thermodynamic analysis of the isobaric-isothermal compression, adiabatic compression, and forced compression of the highly dispersed lyophobic systems, i.e., systems based on zeolites, asbestos, and other capillary-porous substances filled with liquid metals, is presented in Ref. [23]. This thermodynamic approach was extended to the life of coral reefs, which are regarded as a heterogeneous highly dispersed lyophobic system [24], consisting of an open porous rigid matrix coated by lipids, not wetted by the sea water. References [5,6] present the physical basement and the main properties of a colloidal damper, named “heterogeneous structure of the energy accumulation–dissipation.” Design solutions of this kind of damper, with high dissipating capability, are illustrated in [7,21] for different applications such as vehicle suspensions and seismic dampers. The colloidal suspension might be regarded as consisting of repulsive clathrates [21]. Thus, in traditional chemically inert clathrates “AB,” a molecule “A” spontaneously intrudes into a microcavity formed by molecule “B” and remains indefinitely immobilized there, due to the steric obstacles. In the case of repulsive clathrates, liquid cluster “A” is forced to penetrate the cavity “B” of a solid microparticle, thus forming clathrate “AB.” The cluster “A” under the action of repulsive forces may spontaneously leave cavity “B,” producing the expansion of the heterogeneous system, and such repulsive clathrates may be considered as a kind of “molecular” spring [21]. In this work, a design solution from a practical point of view of the CD test rig and the measuring technique of the hysteresis are described. A brief review of the water physical properties relative to the CD concept is presented. Recently, we investigated the influence of the bonding density of the hydrophobic coating on the CD hysteresis [9]. Here, the analysis is completed with the influ-

ence of the length of the grafted molecule, pore diameter, and particle diameter on the CD hysteresis, for distinctive types and mixtures of silica gels. Temperature variation during functioning is recorded and the CD cycle is interpreted from a thermodynamic standpoint. Variation of the CD dissipated energy and efficiency with pressure, water quantity, and relaxation time is illustrated. Experimental results are justified by the analysis of the water flow into the porous matrix, CD thermodynamics, and the mechanism of the energy dissipation.

2. CD test rig

Figure 3 shows a design solution from a practical point of view of the CD test rig. Colloidal suspension is directly introduced into the test chamber (see for comparison solutions proposed by Refs. [6,7,21]), which is located inside the high-pressure cylinder. High-pressure piston (of diameter $D = 20$ mm), thread plugs, and high-pressure gauge close the test chamber. Copper gaskets, "O" ring, and "V" packing assembly are used to seal the experimental chamber, in which can be created a maximum pressure of 120 MPa. The low-pressure cylinder (Taiyo 100S-1R), with a diameter $D_{\mathrm{ha}} = 80$ mm, represents a hydraulic amplifier of the pump pressure with the factor $(D_{\mathrm{ha}}/D)^2$. Static tests, i.e., experiments at low piston velocities (frequencies), are performed by employing a hand pump (Rikken P16B). The piston maximum velocity is given by $v_{\max} = 4q_{\max}/(\pi D_{\mathrm{ha}}^2)$, and for a maximum flow rate delivered by the pump $q_{\max} = 50$ ml/s, one obtains $v_{\max} = 10$ mm/s. The CD cycle can be considered as isothermal until a critical velocity of the piston, which is on order of 20–200 mm/s [5–7,14], as a function of the porous matrix type. For speeds larger than the critical velocity, the cycle becomes quasi-adiabatic [7]. In our experiments, no significant heating occurs, as will be later proved. Nowadays, we are investigating the modification of the CD cycle in the dynamic regime on a test rig, which allows a piston velocity up to 1 m/s (50 Hz maximum frequency), and this research will be the subject of a further communication. Here, data concerning the pressure p (high-pressure gauge, Kyowa PG-2TH), stroke s (displacement sensor, Keyence UD-500), and temperature T (digital thermometer TR2114) are recorded in time t. When the time between pressure and stroke is eliminated, the CD hysteresis is found as a function: $p = p(s)$.

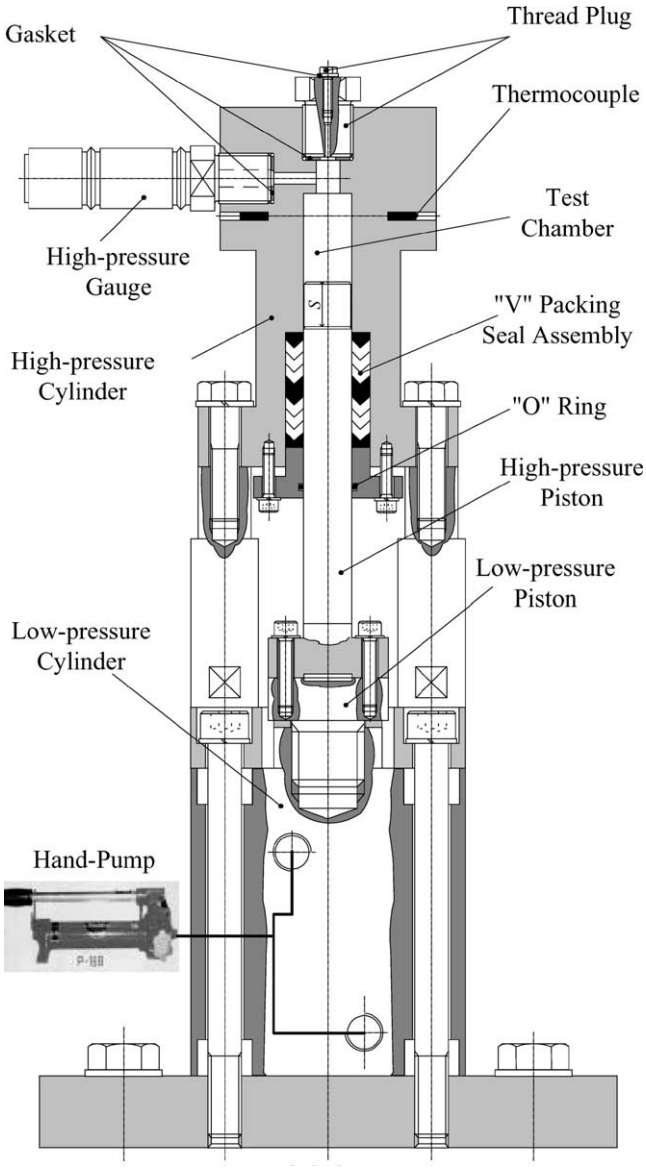


Fig. 3. CD test rig.

3. Materials

3.1. Water

Table 1 presents a brief review of the bulk water physical properties relative to the CD concept, i.e., the variation of the surface tension σ, dynamic viscosity μ_0, change in viscosity with pressure $\partial\mu/\partial p$, density ρ_0, and compressibility c versus temperature T at atmospheric pressure p_0. CD working range of temperatures was considered, 0–80 °C; for

Table 1
Bulk–water data: variation of the surface tension σ, dynamic viscosity μ_0, change in viscosity with pressure $\partial\mu/\partial p$, density ρ_0, and compressibility c versus temperature T at atmospheric pressure p_0

T (°C)	σ (mN/m)	μ_0 (mPa s)	$\partial\mu/\partial p$ (ps)	ρ_0 (kg/m^3)	c (nPa^{-1})
0	75.7	1.792	−2.5	999.8	0.5089
10	74.2	1.307	−1.0	999.7	0.4781
20	72.8	1.002	−0.4	998.2	0.4589
30	71.2	0.797	−0.05	995.7	0.4477
40	69.6	0.653	0.04	992.2	0.4424
50	67.9	0.547	0.08	988.0	0.4417
60	66.2	0.467	0.11	983.2	0.4450
70	64.4	0.405	0.14	977.8	0.4516
80	62.6	0.355	0.17	971.8	0.4614
Refs.	[25,31,39]	[26,28,39]	[28–30]	[39,59]	[1,60]

lower temperatures solutions of water and antifreeze agent can be used [5,6]. Surface tension σ is only a function of the temperature T and can be represented, for example, in the van der Waals form [23–25],

$$\sigma = \sigma_c(1 - T/T_c)^{1.16} \cong \sigma_c(1 - T/T_c), \tag{2}$$

where σ_c is a constant and T_c is the critical temperature at which the surface tension becomes nil. Equation (2) expresses a linear dependence of the surface tension against temperature, the slope being negative: $d\sigma/dT = -\sigma_c/T_c \cong -0.16$ mN/(m K). Usually Barus and Slotte equations [26,27] are used to model the variation of liquids dynamic viscosity against temperature. Recently, Eq. (3) was proposed for water [28], providing impeccable accuracy in the $[-30; 100]$ °C temperature interval,

$$\mu_0(T) = k_1\big[\Delta T + k_2(\Delta T)^2 + k_3(\Delta T)^3 + k_4(\Delta T)^4\big]^{-\gamma}, \tag{3}$$

where $\Delta T = T - T_0$ ($T_0 = 225.334$ K); $k_1 = 883.08 \times 10^{-3}$ Pa s K$^{\gamma}$; $k_2 = 2.28 \times 10^{-3}$ K^{-1}; $k_3 = -1.14 \times 10^{-5}$ K^{-2}; $k_4 = 1.55 \times 10^{-8}$ K^{-3}; $\gamma = 1.57$. Viscosity of liquids increases exponentially with pressure [29,30], as usually expressed by the Barus equation [26,27]. Water below 33 °C is the only exception, in which case it is found that the viscosity first decreases before eventually increasing [26,27]. For moderate pressures ($p < 150$ MPa), the dependence of viscosity versus pressure is almost linear [28]:

$$\mu = \mu(p, T) = \mu_0(T) + \frac{\partial \mu}{\partial p}(p - p_0). \tag{4}$$

Using Table 1 and Eq. (4), one finds the water dynamic viscosity at the room temperature ($T = 20$ °C) and $p = 60$ MPa as being 0.978 mPa s, which means only a 2.4% modification, relative to the viscosity at atmospheric pressure and the same temperature (1.002 mPa s). Thus, for the CD working intervals of pressure and temperature, one should consider the variation of the water viscosity with temperature, but the pressure influence can be neglected. Variation of the water density with pressure can be written as [29]

$$\rho = \rho(p, T) = \rho_0(T)\big[1 + c(p - p_0)\big]. \tag{5}$$

Since at $T = 20$ °C and $p = 60$ MPa the term $c(p - p_0)$ is only about 0.028 (see Table 1 and Eq. (5)), water can be regarded as almost incompressible fluid.

Remarks

It is considered as quite certain that if a film of water with a thickness of 2–3 molecular layers exists on a surface or in a pore, then its behavior and structure will be determined by interactions with the surface and will be entirely different from those of bulk water [31]. On the other hand, the properties of water layers thicker than 1000 nm can be assumed as identical to those of the bulk liquid. Characteristics of water in layers of 1- to 1000-nm thickness are not established yet, but recent evidence indicates that it is likely that the influence of the surface on the water structure does not extend to more than 10 nm [31]. Since the water properties in mesopores are still questionable, in this work the bulk water data will be taken into account. However, we would like to underline the following:

- Some investigators have observed inflections of the surface tension–temperature curve, in the range of 10–20 °C, while others claim that no such inflections exist [31].
- Water viscosity seems to increase very much in small capillaries, being 1.5 times higher than the bulk value in a capillary of radius 50 nm [31]. An 8-nm-thick layer of water on the capillary surface, which is not sheared by the forces causing the liquid flow, could account for this. The effect decreases with increasing temperature and at 70 °C the viscosity of water in pores equals the bulk value [31]. This remark allows better understanding of the water flow in the CD porous matrix.
- Water density for a 3-nm-thick film is only 1% less than that in the bulk liquid [31], consequently, this effect can be neglected.

3.2. Silica gel

We observed that the hydrophobic porous silica gel matrix, suitable for CD, is actually used in modern high-performance liquid chromatography [10–13,32–34]. It was proved [14,19,20] that chemical modification of silica gel with a linear chain of n-alkylchlorosilanes (Fig. 2) was effective in the case of water porosimetry, and the maximum hydrophobicity of the surface was obtained for $n = 16$ (hexadecylsilyl) and $n = 8$ (octylsilyl). In this work, the hydrophobic coating of silica gel was performed with short ($n = 1$, i.e., $-Si(CH_3)_3$ abbreviated C1) and long ($n = 18$, i.e., octadecylsilyl, $-Si(CH_3)_2C_{18}H_{37}$, abbreviated C18) linear chains of alkylsilanes. Modified silica gel particles were provided by Fuji Silysia Chemical Ltd., as customized products.

A revision of the influence of the type and length of the grafted molecule, bonding density, degree of coverage (random, island-like, uniform), pore structure (pore size distribution, dispersion of the pore size distribution), temperature, activator, solvent, etc., on the properties of the hydrophobic layers deposed on silica gels is presented in Ref. [34]. It was proved [32] that passing from a flat to a concave surface (e.g., pore space), the bonding density and the thickness of the bonded layer are determined by the steric hindrance that occurs when the upper parts of the bonded molecules come into contact. Thus, if the pore diameter $2a$ is less than collision diameter D^* (e.g., $D^* = 10.8$ nm for C18 coating), the theoretical bonding density N_{th} and the thickness of the bonded layer h can be calculated as follows [32,34]:

$$N_{\text{th}} = 0.434a, \qquad h = a/3. \tag{6}$$

When the average pore diameter is larger than 14 nm (for C18 coating), the bonded layer has a flexible structure and the bonding density does not depend on the pore diameter,

i.e., $N_{\text{th}} = 2.3$ group/nm^2 and $h = 2.45$ nm. Hydrophobic modification affects (and is affected by) the pore size distribution, the mean pore diameter, the specific surface, and the pore volume [19,32,34–36]. Thus, the specific surface and the bonding density of the alkyl groups can be estimated [19] from the elemental analysis of carbon, using the equations

$$S_{\text{am}} = S_{\text{bm}}\left(1 - \frac{P_c}{100}\frac{M_m}{12n_c}\right),$$
$$N = \frac{600000P_c}{(1200n_c - P_cM_m)S_{\text{bm}}}\ (\text{group/nm}^2), \tag{7}$$

where S_{bm} (m^2/g) and S_{am} (m^2/g) are the specific surfaces of silica gel before (bm) and after (am) modification, P_c (%) is the carbon percentage (by weight) in the silylated silica, n_c is the number of carbon atoms in the grafted molecule, and M_m (g/mol) is the molar mass of a modifier except for an anchor group. The relation between the mean pore diameters of silica gel before and after modification is given by [19,32]

$$(2a)_{\text{am,mean}} = (2a)_{\text{bm,mean}} - 2h. \tag{8}$$

Characteristics (grafted molecule; end-capping; pretreatment conditions; coverage; mean particle diameter $(2b)_{\text{mean}}$; thickness of the bonded layer, h; mean pore diameter $(2a)_{\text{mean}}$, specific surface S and pore volume V_p before and after modification; carbon percentage in the silylated silica P_c; theoretical N_{th} and real N bonding densities) of the studied silica gels (S1–S11) are given in Table 2. Figure 4a presents the particle size distributions of all studied silica gels (S1–S11). Figure 4b illustrates the pore size distribution for silica gels S1, S5, and S6, determined from nitrogen adsorption, using the Cranston–Inkley method [12,16]. These results are obtained for the same type of silica gel (Sylosphere C1504-500) unmodified (S1), C1 coated (S5), and

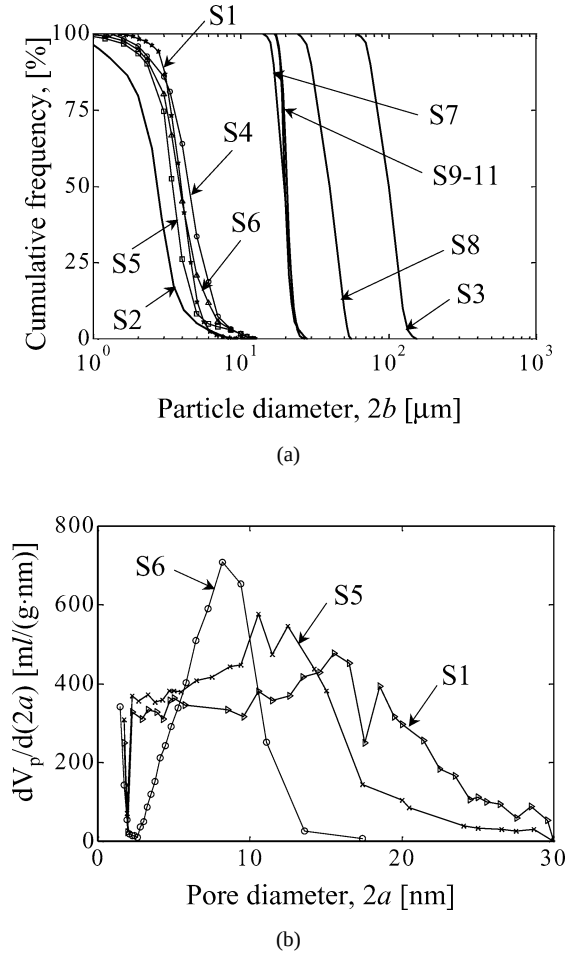


Fig. 4. Particle size (a) and pore size (b) distributions of the studied silica gels.

Table 2
Characteristics of the studied silica gels

Silica gel	S1	S2	S3	S4	S5	S6	S7	S8	S9	S10	S11
Trade name	Sylosphere C1504-500	Sylophobic 100	MB-4B	Sylosphere C1504-77	Sylosphere C1504-4.5	Sylosphere C1504-ODS	ODS-BU 0020MT	ODS-BU 3050MT	ODS-SMB 100-20	ODS-SMB 200-20	ODS-SMB 300-20
Grafted molecule	–	C1	C1	C1	C1	C18	C18	C18	C18	C18	C18
End-capping	–	–	–	–	–	+	+	+	+	+	+
Pretreatment conditions	–	200 °C, 2 h atmosphere	200 °C, 2 h atmosphere	200 °C, 2 h atmosphere	200 °C, 2 h atmosphere	80 °C, 2 h vacuum	80 °C, 2 h vacuum	80 °C, 2 h vacuum	80 °C, 2 h vacuum	80 °C, 2 h vacuum	80 °C, 2 h vacuum
Coverage	–	Random	Random	Random	Relatively uniform	Uniform	Uniform	Uniform	Uniform	Uniform	Uniform
$(2b)_{\text{mean}}$ (μm)	3.9	2.6	100.0	3.9	3.9	3.9	20.0	40.0	20.0	20.0	20.0
$(2a)_{\text{bm,mean}}$ (nm)	13.4	10.0	7.8	13.4	13.4	13.4	10.5	10.5	14.2	25.8	36.2
h (nm)	–	0.30	0.30	0.30	0.30	2.23	1.75	1.75	2.40	2.45	2.45
$(2a)_{\text{am,mean}}$ (nm)	–	9.4	7.2	12.8	12.8	8.9	7.0	7.0	9.4	20.9	31.3
S_{bm} (m^2/g) (N_2)	380	343	471	380	380	380	328	320	300	150	100
S_{am} (m^2/g) (N_2)	–	336	450	350	346	269	250	245	226	129	90
$V_{p,\text{bm}}$ (ml/g)	1.257	1.462	0.961	1.257	1.257	1.257	1.116	1.089	1.074	1.021	0.951
$V_{p,\text{am}}$ (ml/g)	–	1.331	0.783	1.093	1.032	0.763	0.413	0.405	0.532	0.607	0.635
P_c (wt%)	–	1.00	2.21	3.93	4.36	22.57	18.40	18.10	19.00	10.83	7.57
N_{th} (group/nm^2)	–	2.17	1.69	2.30	2.30	2.30	2.28	2.28	2.30	2.30	2.30
N (group/nm^2)	–	0.49	0.82	1.87	2.10	2.10	1.84	1.85	2.10	2.10	2.10

C18 coated (S6). As expected [34–36], one observes that the hydrophobic treatment affects the mean pore diameter (see Table 2), in agreement with Eq. (8), and this correction will be useful in the analysis of the CD experimental results.

4. Results and discussion

4.1. Influence of the bonding density and the length of the grafted molecule

Figure 5 presents the influence of the bonding density and the length of the grafted molecule on the CD hysteresis. In the case of the colloid based on hydrophilic silica gel S1 (Fig. 5a, $N = 0.00$) one obtains the same small hysteresis as for the pure water. This negligible hysteresis occurs due to the air bubbles, always present in the real water. CD has poor efficiency in such circumstances since the water inherently enters and rests captive inside the porous matrix. Consequently, the surface modification is essential for achieving an effective CD. In the case of silica gel S2 (Fig. 5b, $N = 0.49$) one obtains an irreversible, small 1st hysteresis, i.e., the 2nd hysteresis becomes negligible. For silica gel S4 (Fig. 5d, $N = 1.87$) an irreversible, large 1st hysteresis is recorded. The 1st cycle shown in Fig. 5c (silica gel S3, $N = 0.82$) occurs as an intermediate case between silica gels S2 and S4. In the case of silica gel S5 (Fig. 5e,

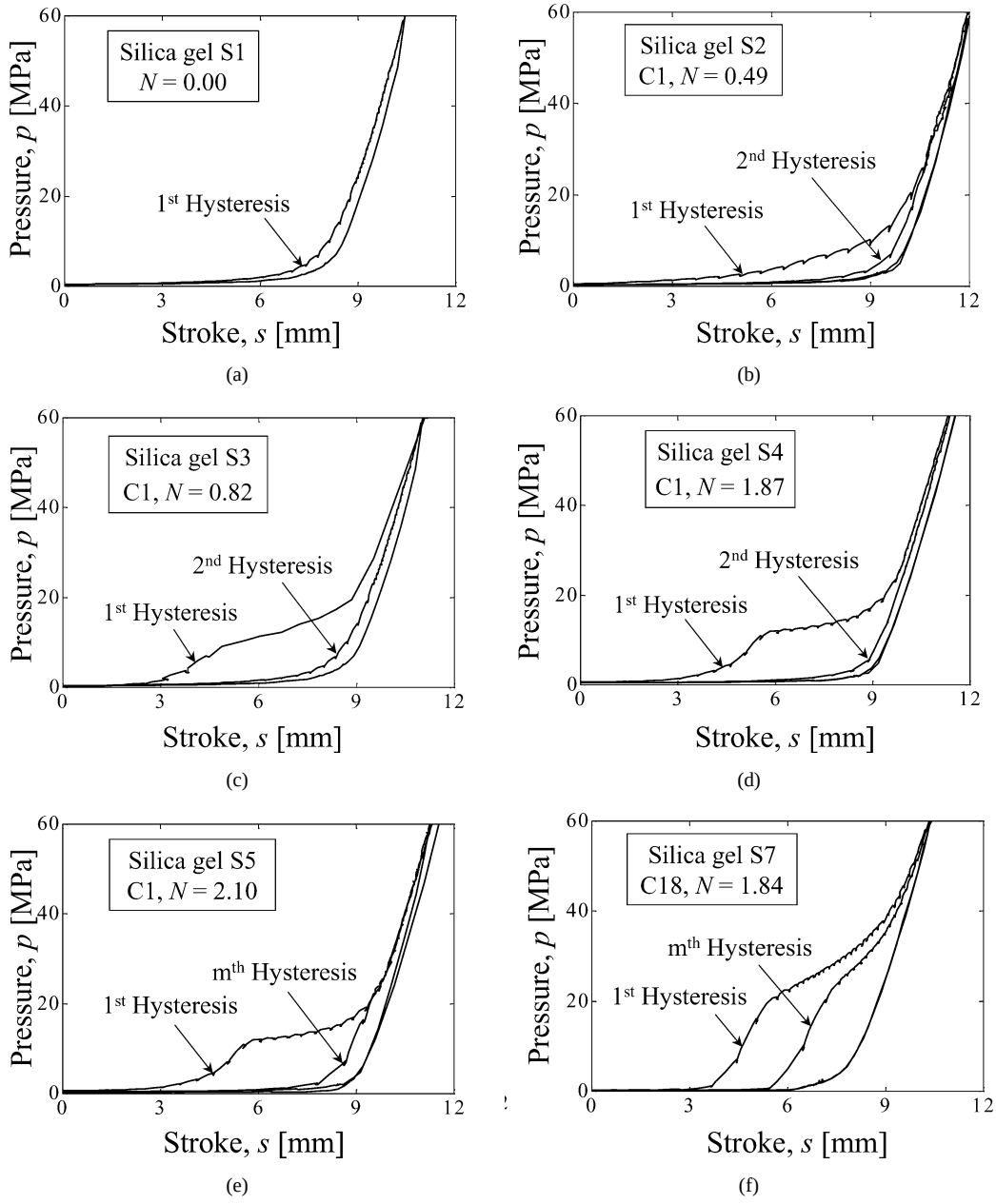


Fig. 5. Influence of the bonding density and length of the grafted molecule on the CD hysteresis ($m = 25$).

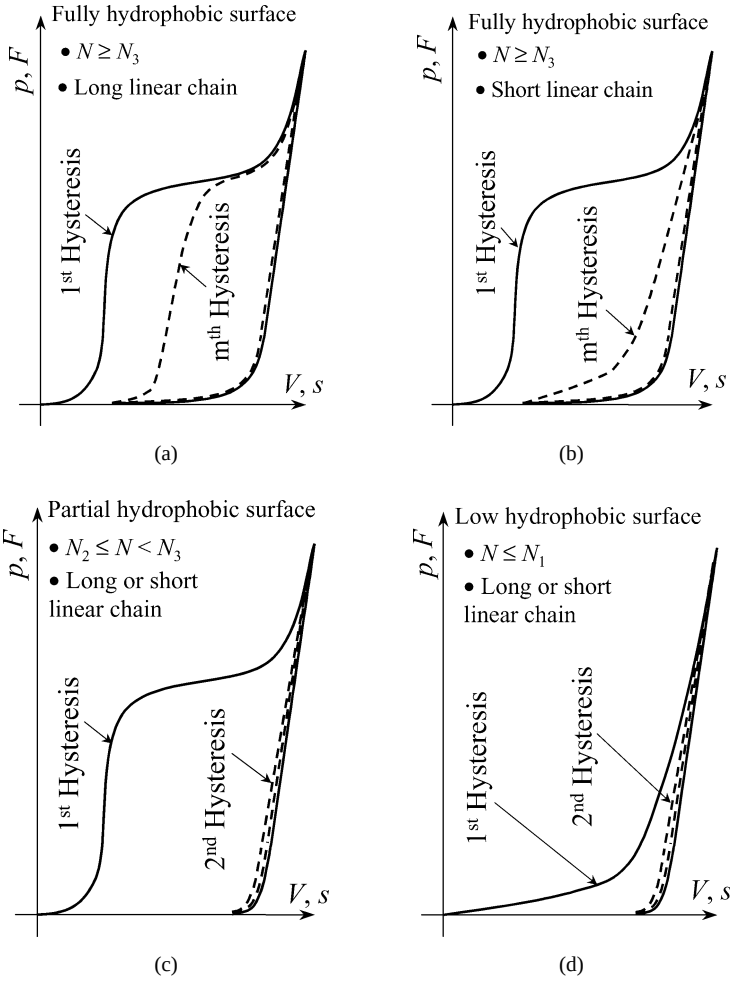


Fig. 6. Influence of the silica gel modification on the water hysteresis.

$N = 2.10$), the 1st large hysteresis is followed by small, but repetitive cycles (2nd–mth). Finally, for silica gel S7 (Fig. 5f, $N = 1.84$), the 1st large hysteresis is succeeded by relatively large and repetitive cycles (2nd–mth). These results are generalized in Fig. 6, and they agree with data obtained for water porosimetry [14,19,20]. Thus, the CD hysteresis seems to be strongly influenced by the bonding density and the length of the alkyl chain, as follows:

- For a low hydrophobic surface ($N \leqslant N_1$), both for a long or short grafted molecule (Figs. 5b and 6d), a small irreversible 1st cycle occurs. This case has no practical importance from a damping standpoint.
- For a partial hydrophobic surface ($N_2 \leqslant N \leqslant N_3$), both for a long or short grafted molecule (Figs. 5c, 5d, and 6c), an irreversible, large 1st cycle is recorded. In this case CD can be used as a shock absorber.
- For a fully hydrophobic surface ($N \geqslant N_3$), modified by a short alkyl chain (C1), the 1st large hysteresis (Figs. 5e and 6b) is followed by small, but repetitive cycles (2nd–mth). With use of a long alkyl chain (C18), the 1st large hysteresis (Figs. 5f and 6a) is succeeded by relatively large and repetitive cycles (2nd–mth). Here, $m = 25$, but as will be later proved, the hysteresis is reproducible for at least thousands of cycles. In this case CD can be used for vibration reduction [5–7,9,21].

The following values of the bonding densities, which determine the cycle type, were suggested [14]: $N_1 \cong 0.5$ group/nm^2, $N_2 \cong 1.0$ group/nm^2, and $N_3 \cong 2.0$ group/nm^2. Results presented in Fig. 5 generally agree with these limits.

To explain the influence of the length of the grafted molecule (Figs. 5 and 6), one performs a differential thermal analysis (DTA-TG) of silica gels S5 and S6 (Fig. 7), which have the same initial structure (silica gel S1) and the same bonding density (Table 2). The difference between them is the length of the alkylsilane chain used for the hydrophobic modification, which is short (C1) for silica gel S5 and long (C18) for silica gel S6. Four probes, each 9.9 mg, were prepared as follows: silica gel S5 (C1), BE; silica gel S5 (C1), AE; silica gel S6 (C18), BE; silica gel S6 (C18), AE. Abbreviation BE means before experiment in the CD test chamber, i.e., the probe consists only of silica gel S5 or S6. Abbreviation AE means after experiment in the CD test chamber, at 60 MPa pressure. In this case the probe represents the colloidal suspension of silica gel S5 or S6 and water, collected

from the test chamber (Fig. 3). The probes are successively introduced into a resistance oven (Rigaku, Thermo plus TG8120), which provides a heating rate of 10 °C/min in the temperature range 20–500 °C. Figure 7a displays the weight loss TG variation versus temperature and Fig. 7b shows the DTA modification against temperature. In the case of BE probes, water evaporation cannot be detected in the temperature range 20–120 °C, i.e., the hydrophobic modification was successfully done and the silica gel is free of water. At 220 °C occurs the vaporization of the C18 coating (silica gel S6) and at 450 °C starts the vaporization of the C1 coating (silica gel S5). In conclusion, from a thermal standpoint, the C1 coating is more stable than the C18 one. Considering the AE probes, in the 20–120 °C temperature interval occurs the water evaporation: 5.5 mg of water for silica gel S5 and 5.8 mg of water for silica gel S6. Consequently, the real mass of silica gel is 4.1 mg for S6 and 4.4 mg for S5, i.e., 41%, respectively, 44% from the total mass of the probe. Around 220 °C occurs the vaporization of the C18 coating (silica gel S6) and at 460 °C takes place the vaporization of the C1 coating (silica gel S5). Since the peak of silica gel S6 (at 220 °C) after experiment (AE) is about 41% of the peak before experiment (BE), one concludes that the C18 coating was not affected by high pressure. In contrast, the peak of silica gel S5 (around 460 °C) after experiment (AE) is much less than 44% of the peak before experiment (BE); i.e., the C1 coating was partially damaged by the high pressure. In conclusion, from the standpoint of pressurization, the C18 coating is more stable than the C1 one.

4.2. Influence of the mean pore diameter and the mean particle diameter

Figure 8a presents the 1st cycle obtained for silica gels S9, S10, and S11, which have the same particle size distribution but different mean pore diameters $(2a)_{\mathrm{am,mean}}$, i.e., about 10, 20, and 30 nm (see Fig. 4a and Table 2). Neglecting the gas pressure p_g in Eq. (1), for a contact angle $\theta = 130°$, one finds the mean adsorption pressures: 20 MPa for S9, 9 MPa for S10, and 6 MPa for S11, which agree with the experimental data (Fig. 8a). These results prove that the adsorption pressure equals the Laplace capillary pressure, as assumed in Eq. (1) and Fig. 2. The gas pressure p_g is found as negligible and, later, a detailed discussion concerning this aspect will be made. Figure 8b illustrates the 1st hysteresis obtained for silica gels S7 and S8, which have the same mean pore diameter but different mean particle

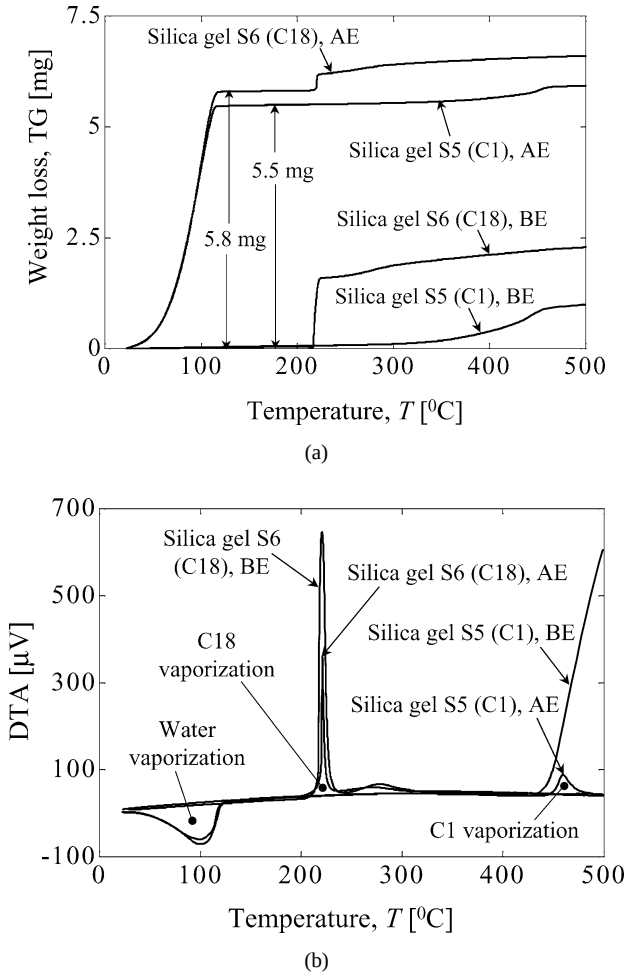


Fig. 7. DTA-TG analysis for silica gels S5 and S6; TG versus temperature (a) and DTA versus temperature (b).

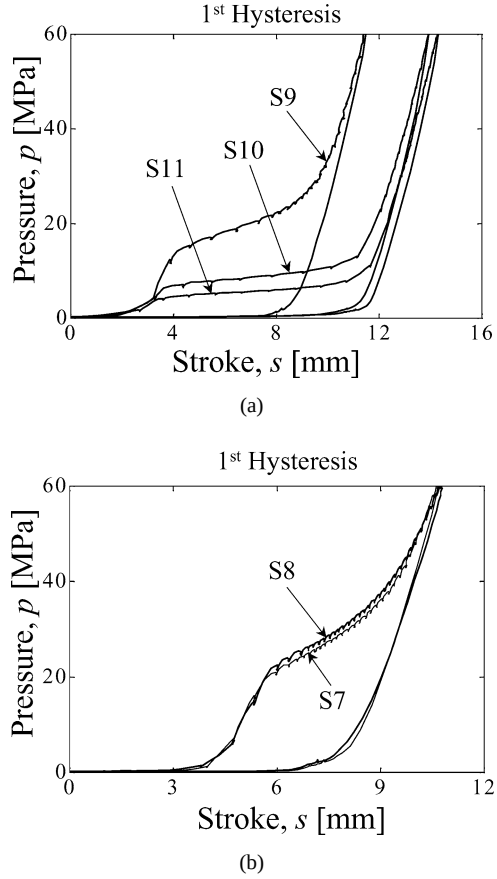


Fig. 8. Influence of the mean pore diameter (a) and the mean particle diameter (b) on the CD hysteresis.

diameters $(2b)_{\text{mean}}$, i.e., 20 and 40 μm (see Fig. 4a and Table 2). The cycles are almost superposed, consequently, the mean particle diameter, and implicitly the interparticle volume has no influence on the CD hysteresis. This can be explained by the theory of packed particles [10,37]. Thus, for packing of spheres of diameter $2b$, the radius of the circle inscribed in throats varies between $0.155b$ (hexagonal packing) and $0.414b$ (cubic packing). Taking, for instance, $b = 10$ μm, the minimum throat radius is about 1.55 μm, and its corresponding adsorption pressure is on order of 0.01 MPa, i.e., negligible.

4.3. Influence of the loading pressure and temperature

Figures 9a and 9b show the influence of the maximum loading pressure on the CD 1st and mth hysteresis, obtained for $M = 4$ g of silica gel S7, at 20 °C. Area of the hysteresis, which represents the CD dissipated energy, increases with the increasing pressure. The 1st hysteresis is considerably larger than the following cycles, which are identical. Figure 9c presents the CD hysteresis obtained at progressive loading, for $M = 4$ g of silica gel S7, at 20 °C. During this kind of experiment, the pressure is successively increased at 25, 30, 40, 51, and 60 MPa. After each loading, the pressure is released at zero. Figure 9d illustrates the 2nd, 600th, and 1200th hysteresis, obtained for $M = 4$ g of silica gel S7, at a loading frequency of 0.1 Hz. The temperature increases from 20.4 to 25.2 °C, the heating being about 0.004 °C/cycle. Consequently, for small piston velocities (frequencies) the cycle can be considered isothermal [7,14]. Shape of the mth hysteresis does not change since the water surface tension has a small variation (only 1%) in this temperature range (see Table 1). To explain the isothermal behavior of the CD cycle, one performs an analysis of the water flow into the porous matrix, followed by a thermodynamic analysis.

4.3.1. Flow analysis

In this section one considers the following assumptions:

- Silica gel presents identic cylindrical pores, one end being opened and the other closed.
- Water flowing into the pore space obeys the Navier–Stokes equations, the continuity equation, the no-slip condition on the solid wall, the free surface condition at the water–gas interface (which is a meniscus at the front), and the entry condition at the interface of the bulk–water and the pore. The no-slip condition on the solid wall will be later discussed in detail.
- At the pore entry the velocity profile (Fig. 10) is a uniform one of potential flow ($u = $ ct.). As the flow advances, a Poiseuille regime develops, and then in the neighborhood of the front, the velocity profile follows the meniscus shape (surface tension regime, Fig. 10). Modification of the velocity profile can be considered by

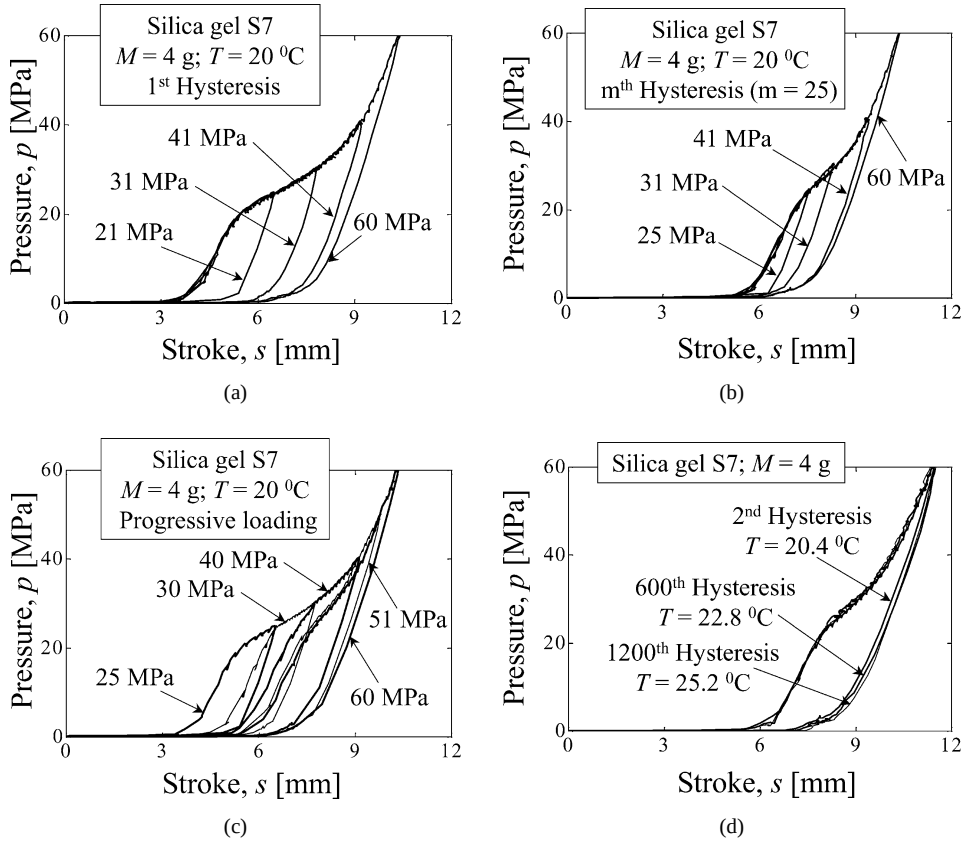


Fig. 9. Influence of the loading pressure and temperature on the CD hysteresis (silica gel S7; $M = 4$ g).

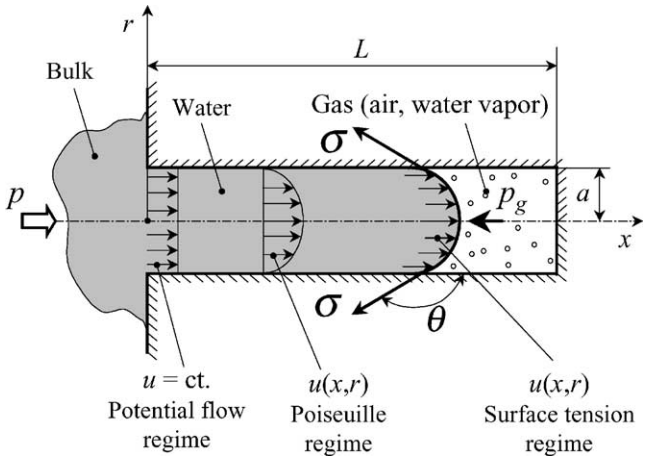


Fig. 10. Model of water flow in the pore space.

including additional resistance to the known solution of the Poiseuille flow [38], but these effects are neglected here.

- Water is considered as a Newtonian incompressible fluid, as discussed in Section 3.1.
- Water flow into the pore space is isothermal, as already discussed. It can also be categorized as creeping and laminar. This statement is justified by the very small value of the Reynolds number $Re = 2\rho u_m a/\mu$ [39,40], which is about $10^{-10} \cong 0$. To estimate the Reynolds number, one first calculates the mean length of the pore $L = aV_{p,\mathrm{am}}/(aS_{\mathrm{am}} - 2V_{p,\mathrm{am}})$, which for silica gel S7 is about $L = 30$ nm (see Table 2). The surface of the pores ends, opened to the water penetration, can be written as $S_p = V_{p,\mathrm{am}}/L = S_{\mathrm{am}}/(1 + 2L/a)$, which for silica gel S7 is about $S_p = 14$ m^2/g. Then, the mean velocity of the water penetrating the pore space is obtained from the flow rate conservation inside of the CD cylinder as $u_m = \pi D^2 v_{\max}/(4MS_p)$, which for $M = 4$ g of silica gel S7 is about $u_m = 56$ nm/s. Consequently, the water flow into the pore space is very slow, and such flows are named creeping flows [39–44]. In these circumstances, the inertial terms can be neglected in comparison with the viscous terms.

The Newtonian equation of the water motion into the pore space is given by [38]

$$(M_0 + \rho_0 \pi a^2 x)\frac{du_m}{dt} = 2\pi a\sigma\cos\theta - R(x, u_m), \tag{9}$$

where M_0 is the added mass of the fluid and $R(x, u_m)$ is the total resistance to the flow, which comes from the wall shear stress due to the viscosity of the fluid. Definition of M_0 is that when the mean velocity of the fluid at the enter section ($x = 0$) is u_m, the kinetic energy of the fluid in the entire bulk is exactly $M_0 u_m^2/2$. The importance of the added mass M_0 can be emphasized by the observation that if $M_0 = 0$, the initial acceleration would be infinite and the beginning of the motion would be indefinite. For a cylindrical tube of radius a, the added mass can be taken as $M_0 = 3\pi\rho_0 a^3/8$ [38]. From the known solution of Poiseuille flow in cylindrical ducts [38,39], one calculates the resistance as $R(x, u_m) = -\pi a^2(p - p_g)$, where the pressure of the gas, captive in the pore, can be expressed from its isothermal compression $p_g = p_0 L/(L - x)$. Next, Eq. (9) can be written in dimensionless form as

$$\Gamma\left(\frac{3}{8} + \bar{x}\right)\frac{d^2\bar{x}}{d\bar{t}^2} = 2\bar{\sigma}\cos\theta + \bar{p} - \frac{\bar{L}}{\bar{L} - \bar{x}}, \tag{10}$$

where $\bar{x} = x/a$, $\bar{L} = L/a$, $\bar{p} = p/p_0$, $\bar{\sigma} = \sigma/(ap_0)$, $\bar{t} = t/t_c$, and $\Gamma = \rho_0 a^2/(p_0 t_c^2)$. Taking for the compression time t_c values on order of 10–10^{-2} s (compression frequency about 0.1–100 Hz), one finds a dimensionless number Γ on order of 10^{-21}–10^{-15}. Thus, it becomes possible to neglect the inertia term, i.e., the left side of Eq. (10), and this result was anticipated by the observation that $Re \cong 0$. In other words, the Newtonian equation of the water motion into the pore space reduces to Eq. (1). Besides, considering an external pressure $p = 60$ MPa, the gas pressure p_g becomes 10% of p, when $x \geqslant 0.98L$; i.e., only when the pore is almost filled with water does the gas pressure take values comparable to the external or Laplace pressures. For this reason in Section 4.2 the contribution of the gas pressure p_g was found to be negligible.

Next, one explains why the water flowing into the mesopores space does not heat. Rate of mechanical energy dissipation during any fluid flow may be found by integrating the local dissipation rate Φ over the fluid domain [39,42,43]:

$$Q = \int_V \Phi\, dV. \tag{11}$$

It represents the work done on fluid in overcoming the internal friction; hence, this energy is lost from the mechanical system and appears as heat [39,42,43]. First, one should bear in mind the theorem of Helmholtz, which stated that the energy dissipation in a creeping flow is less than in any incompressible, continuous motion consistent with the same boundary conditions. For a no-slip Poiseuille flow, as already assumed, the rate of energy dissipation and the heat are given by [39,42]

$$\Phi = \frac{r^2}{4\rho\mu}\left(\frac{dp}{dx}\right)^2, \qquad Q^{\text{no-slip}} = -\pi a^2 L u_m\left(\frac{dp}{dx}\right), \tag{12}$$

where dp/dx is the pressure gradient. We have the opportunity here to reconsider the assumption of no-slip condition on the solid wall. Helmholtz is often credited with finding some evidence of slippage between the boundary of a solid and a liquid flowing over it [42,45]. These results have been extensively criticized and the significance of hydrophobization for the slip phenomenon does not seem to be recognized at this early stage. The matter was revised and the first reliable results for water were those obtained by Schnell [46]. He experimentally detected slippage of water in glass capillaries, treated with vapor of dimethyldichlorosilane, to make them water-repellent. Churaev et al. [47] also reported the

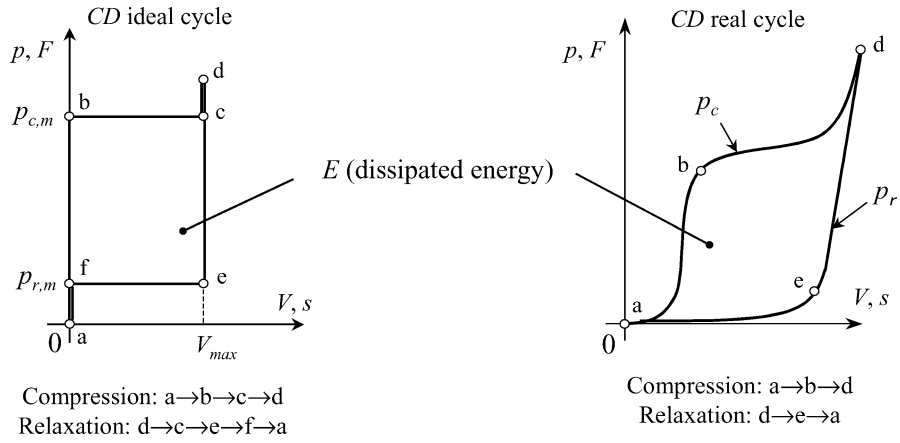


Fig. 11. Ideal and real cycles of CD.

slippage for water in very narrow silica capillaries, treated with trimethylchlorosilane. Thus, it is possible to conclude that there is evidence to suggest that slippage may occur in aqueous systems where the walls are hydrophobic. Slip means that the liquid loses adhesion with the wall and slides over the surface, with a velocity u_s. There is a thin layer (the hydrophobic coating) bonded to the wall, which does not slip, but acts as a lubricant for the more viscous core fluid, so that the latter appears to slip [22,31,48]. In this case the heat becomes [39,42]

$$Q^{\text{slip}} = -\pi a^2 L(u_m - u_s)\left(\frac{dp}{dx}\right). \tag{13}$$

Note that for slip velocity close to the mean speed $u_s \cong u_m$, the heat occurs as negligible since the velocity profile is uniform as in the case of potential flow. Slip occurs when the assumption of the continuous medium is not satisfied [39, 40,42,43], and the main parameter involved is the Knudsen number $Kn = L_p/L$, where L_p represents the molecular free path. If $Kn < 0.01$, the medium can be considered as continuous. For $0.01 < Kn < 0.1$, the fluid flow still preserves the characteristics of a continuous medium, but slippage occurs. Based on the results obtained through Monte Carlo and molecular dynamics simulations [41,48–50], it was suggested [22] that, inside the mesopores, water presents a stratiformly arranged structure of clusters, which flow at high Knudsen number, with boundary and interlayers slip. However, a detailed discussion lies beyond the purpose of this section.

4.3.2. Thermodynamic analysis

To complete the energetic aspects connected to CD, the first law of thermodynamics [51–54] is written for the closed thermodynamic system from Fig. 1b,

$$\Delta U = Q + W, \tag{14}$$

where ΔU is the internal energy variation, Q is the heat exchange with surroundings ($Q > 0$ means that heat is transferred from the surroundings to the CD), and W is the mechanical work ($W > 0$ means that work is done on the CD by the surroundings). Thus, the dissipated energy of shock and vibration E (Fig. 11) equals the mechanical work ($E = W$). First, one considers the CD as a "black box," able to develop a quasi-isothermal cycle. Compression work W_c equals the absorbed energy E_a, which can be written as [1]

$$E_a = W_c = \begin{cases} p_{c,m} V_{\max}, & \text{ideal-cycle,} \\ \frac{\pi D^2}{4} \int_0^{s_{\max}} p_c \, ds, & \text{real-cycle.} \end{cases} \tag{15}$$

Dissipated energy of shock and vibration (Fig. 11) equals the variation of the mechanical work during a cycle and can be calculated as [1,2,9,19,21,22]:

$$E = W = \begin{cases} (p_{c,m} - p_{r,m}) V_{\max}, & \text{ideal-cycle,} \\ \frac{\pi D^2}{4} \int_0^{s_{\max}} (p_c - p_r) \, ds, & \text{real-cycle.} \end{cases} \tag{16}$$

Damper efficiency (capability to dissipate the energy) η (%) is defined as [1,2]

$$\eta = 100 \frac{E}{E_a} = \begin{cases} 100(1 - p_{r,m}/p_{c,m}), & \text{ideal-cycle,} \\ 100 \int_0^{s_{\max}} (p_c - p_r) \, ds \Big/ \int_0^{s_{\max}} p_c \, ds, & \text{real-cycle.} \end{cases} \tag{17}$$

Note that HD maximum efficiency (Fig. 1a) can be expressed as [1,2] $\eta_{\text{HD}} = 100[1 - (d/D)^2]$. Considering the makers recommendation [1] concerning the diameter of the piston rod, $d = 0.7D$, one obtains that the HD efficiency is lower than 51%, and in actual applications is about 30–40%.

Using Eqs. (16) and (17) for the cycles presented in Figs. 9a–c, one obtains the variation of the CD dissipated energy and efficiency versus pressure for $M = 4$ g of silica gel S7, at $T = 20\,^{\circ}\text{C}$ (Figs. 12a and 12b). Curves for progressive loading start on the 1st hysteresis curves and end on the mth hysteresis curves. Energy of the mth hysteresis is about 50% of the 1st hysteresis energy and a detailed discussion concerning this feature will be later given. Maximum efficiency of the 1st and mth hysteresis (76 and 54%) is obtained for the optimum pressure (30 and 40 MPa). Similar results are obtained for $M = 2.5$ g of silica gel S6 (Figs. 12c and 12d) and S5 (Figs. 12e and 12f),

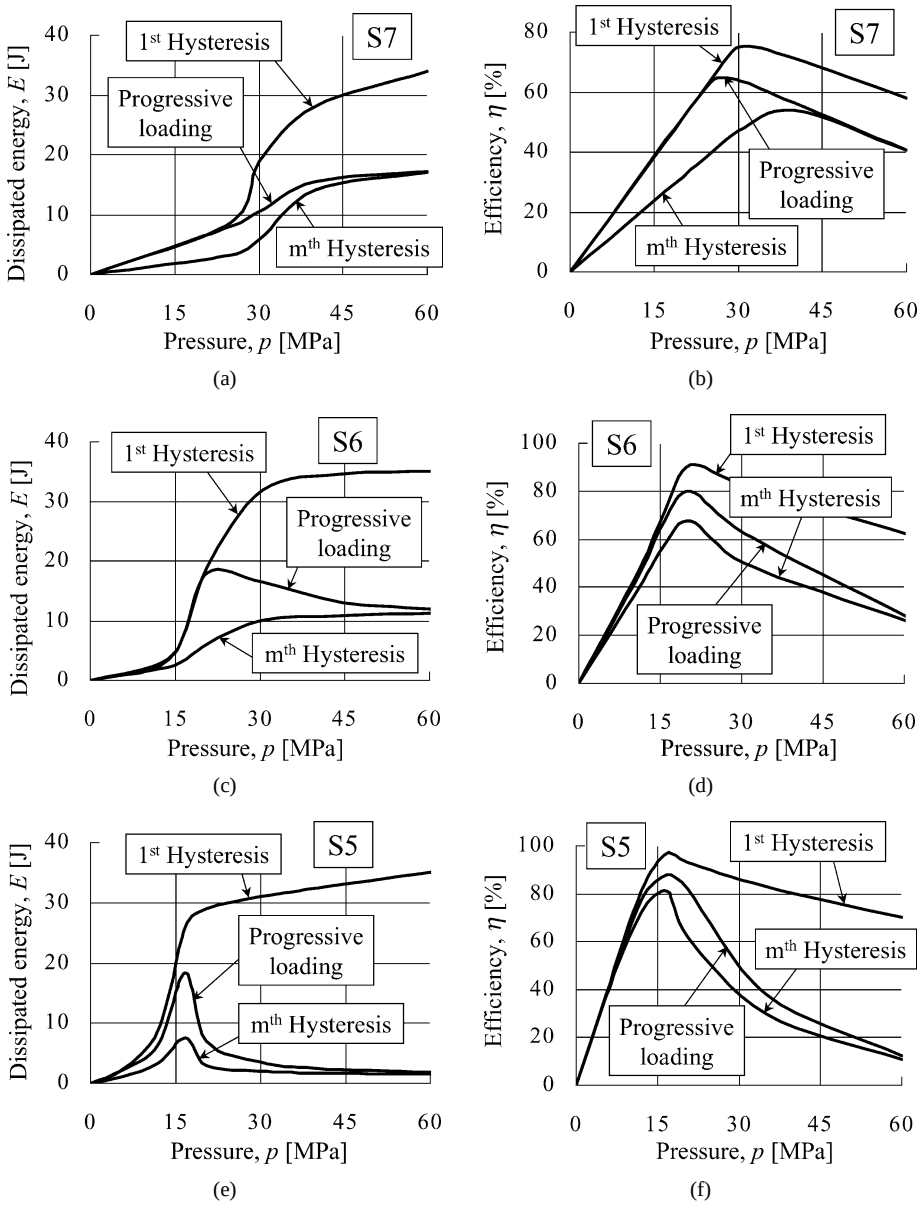


Fig. 12. CD dissipated energy and efficiency for the 1st hysteresis, at progressive loading and for the mth hysteresis: silica gel S7 (a, b); silica gel S6 (c, d); silica gel S5 (e, f).

at $T = 20\,^{\circ}\mathrm{C}$. Energy of the 1st hysteresis has similar variation with pressure for C1 and C18 coatings. For silica gel S5 (Fig. 12e), the energy of the mth hysteresis increases with the pressure increasing, until an optimum value ($p =$ 16.5 MPa), and then decreases. At higher pressure (larger than 25 MPa) the mth hysteresis almost disappears. This means that the water rests captive inside of the porous matrix and the capillary force is not able to push it out during relaxation. On the other hand, for silica gel S6 (Fig. 12c), the energy of the mth hysteresis displays a variation against pressure, similar with that of the 1st hysteresis, i.e., the energy continuously increases with the pressure. At 60 MPa, the energy of the mth hysteresis is about 30% of the 1st hysteresis energy. Concerning the CD efficiency, C1 and C18 coatings show similar tendencies (Fig. 12). Note that the CD maximum efficiency (97%) obtained in the case of the 1st hysteresis of silica gel S5 is about 2 times higher than the maximum efficiency of HD. Our results concerning the CD efficiency (see Eq. (17)) agree with the previous findings: $p_{r,m}/p_{c,m} = 0.05$–0.2 [14,19].

Next, one considers the CD as a heterogeneous system consisting of a porous matrix, water, and gas (air and water vapor), having the interface solid–liquid–gas (Figs. 2 and 10). For a reversible process, involving infinitesimal changes [53], Eq. (14) can be written in the differential form $dU = dQ + dW$, where dQ and dW stands for infinitesimally small amounts of heat and work, given to the system. Volume work is expressed by $dW = -p\,dV$, where p represents the external pressure and $dV = \pi D^2\,ds/4$ is the volume variation (Fig. 1b).

Change in the internal energy occurs due to the solid (S), liquid (L), gas (G), and interface (Σ) contributions: $dU = dU^{\mathrm{S}} + dU^{\mathrm{L}} + dU^{\mathrm{G}} + dU^{\Sigma}$. Under the following assumptions: both water and porous matrix are incompressible; the cycle is isothermal; no chemical reactions and no phase transitions occur in the system; the amount of the colloidal suspension is constant (perfect seals of the test chamber, in Fig. 3), the variation of the internal energy reduces to [23,53]

$$dU = dU^{\Sigma} = T\,dS^{\Sigma} + \sigma\cos\theta\,d\Omega = 0, \tag{18}$$

where S^{Σ} is the interface entropy, σ is the surface tension of the water–gas interface, T is the temperature, θ is the contact angle, and Ω is the area of the water–solid contact interface. Heat exchanged by CD with the surroundings can be written as [39]

$$dQ = T\,dS = T\left[\left(\frac{\partial S}{\partial T}\right)_V dT + \left(\frac{\partial S}{\partial V}\right)_T dV\right], \tag{19}$$

and taking $(\partial S/\partial V)_T = (\partial p/\partial T)_V$, one finds for an isothermal process ($dT = 0$)

$$dQ = T\left(\frac{\partial p}{\partial T}\right)_V dV. \tag{20}$$

Introducing the external pressure (Eq. (1)) into the expressions of the infinitesimal work and heat, and considering the relation between the infinitesimal surface and volume ($d\Omega = 2\,dV/a$), one finds

$$dW = \sigma\cos\theta\,d\Omega - p_g\,dV,$$
$$dQ = -T\frac{d\sigma}{dT}\cos\theta\,d\Omega + p_g\,dV. \tag{21}$$

The first term of dW represents the interfacial work, and the second one is the volume work of the gas isothermal evolution, which represents a secondary effect since the gas pressure is negligible. Thus, CD occurs as a system able to transform the volume work ($-p\,dV$), i.e., the energy of shock and vibration, into the interfacial work ($\sigma\cos\theta\,d\Omega$). The first term of dQ represents the latent heat of isothermal formation of the interface and the second one occurs as the heat of the gas in its isothermal evolution. Since the internal energy variation is nil ($dU = 0$), it results in the equality of work and heat ($dW = -dQ$). Equations (18) and (21) allow the thermodynamical interpretation of the CD cycle [23,24]. An infinitely small compression ($dp > 0$) causes a proportional increase of the interface area ($d\Omega > 0$). Since $d\sigma/dT < 0$ (Section 3.1), heat is supplied from the surroundings ($dQ > 0$) for the isothermal surface extension. At relaxation ($dp < 0$), the system expands and the interface area decreases ($d\Omega < 0$). Latent heat of the isothermal shrinking of the interface is transferred from the system to the surroundings ($dQ < 0$). A similar thermodynamic analysis can be developed in the case of fast compression (high working frequency) when the CD cycle becomes quasi-adiabatic [24].

4.4. Influence of the water quantity

Figure 13 presents the variation of the CD dissipated energy and efficiency versus dimensionless volume ($V_{\mathrm{s}}/V_{\mathrm{w}}$) for the 1st cycle of silica gel S5, at $p = 60$ MPa and $T = 20\,^{\circ}\mathrm{C}$ (V_{w} represents the water volume and V_{s} is the silica gel volume). Maximum dissipated energy and efficiency are obtained for $V_{\mathrm{s}}/V_{\mathrm{w}} = 3.1$, which corresponds to $M = 3$ g of silica gel and $V_{\mathrm{w}} = 3.1$ ml of water. In other words, the optimum volume of water is $V_{\mathrm{w}}/M = 1.033$ ml/g and it equals the pore volume of the silica gel matrix ($V_{p,\mathrm{am}} = 1.032$ ml/g in Table 2). This can be explained from a physical standpoint as follows: for small quantities of silica gel, an excess of water rests in the test chamber after pore filling; on the other hand, for large quantities of silica gel, a deficit of water occurs in the test chamber, and the pores are only partially filled. Thus, the optimum quantity of water should equal the pore volume of the silica gel matrix.

4.5. Influence of the mixtures of silica gels

Figure 14 presents the CD hysteresis obtained for silica gels S5, S6, and their 1:1 mixture ($M = 2.5$ g, $T = 20\,^{\circ}\mathrm{C}$). Mean compression pressure of silica gel S6 ($p_{c,m} \cong 21$ MPa)

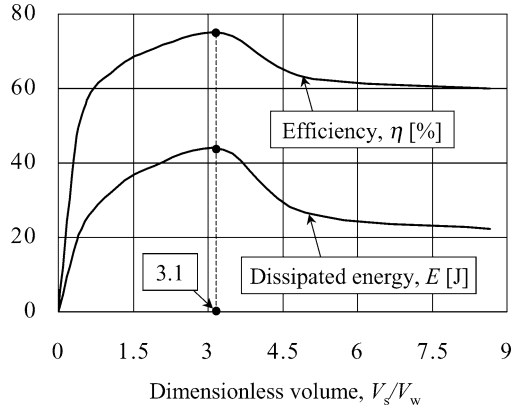


Fig. 13. CD dissipated energy and efficiency versus dimensionless volume ($V_{\mathrm{s}}/V_{\mathrm{w}}$).

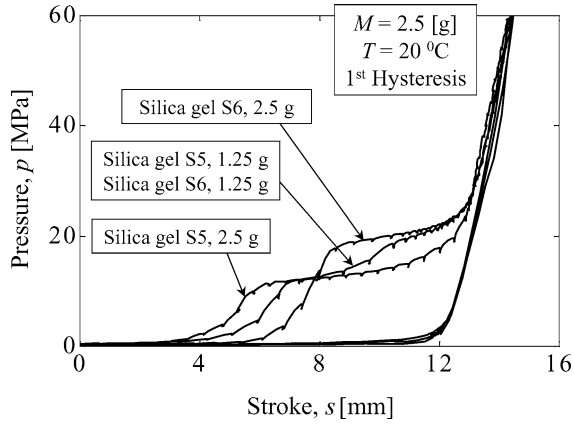


Fig. 14. CD hysteresis for silica gels S5, S6 and their 1:1 mixture.

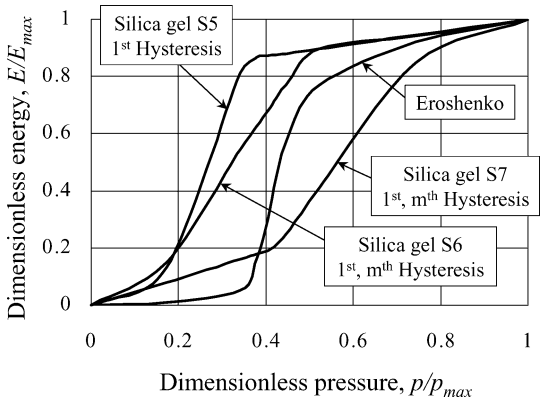


Fig. 15. CD dimensionless energy versus dimensionless pressure.

is higher than that of silica gel S5 ($p_{c,m} \cong 13$ MPa) since the mean pore radius is smaller in the case of silica gel S6 (see Table 2). One observes that the hysteresis of the mixture occurs between the cycles of the two components, as a linear combination. These results prove that when silica gels are mixed with different hydrophobic modification and/or particle architecture, the hysteresis shape can be controlled.

4.6. Comparison with the previously published experimental data

Figure 15 presents the dimensionless energy versus dimensionless pressure for silica gel S5 (1st hysteresis) and silica gels S6 and S7 (1st and *m*th cycle). Note that the curves for the 1st and *m*th hysteresis are coinciding for the C18 grafted molecule. Our results show the same tendency as Eroshenko's results [6]; the discrepancies can be attributed to the different architecture of the porous matrix. Eroshenko's silica gel and the silica gel S5 (C1 modification) display parallel central zones; also the silica gels S6 and S7 (C18 coating) show such parallel central zones. Consequently, the slope of the central zone of the curve of dimensionless energy versus dimensionless pressure is related to the length of the molecule used for the hydrophobic coating.

4.7. Influence of the relaxation time

Figure 16 present the influence of the relaxation time R on the CD 1st hysteresis (a) and *m*th hysteresis (b) for $M = 4$ g of silica gel S7, at $T = 20\,^{\circ}$C. In this experiment, for $R = 0$ (Fig. 16a) the largest 1st hysteresis is obtained, followed by 2nd–*m*th cycles (Fig. 16b), which practically coincide. CD rests for a certain period of time (relaxation time R), and then the experiment is repeated. The 1st hysteresis after the relaxation period (Fig. 16a) is larger than the *m*th cycle, but smaller than the 1st cycle obtained at $R = 0$; it is followed by the 2nd–*m*th cycles (Fig. 16b), which are superposed. The area of the 1st hysteresis increases with the relaxation time, until $R = 17$ h; after that the effect is negligible. In other words, the CD hysteresis has the ability

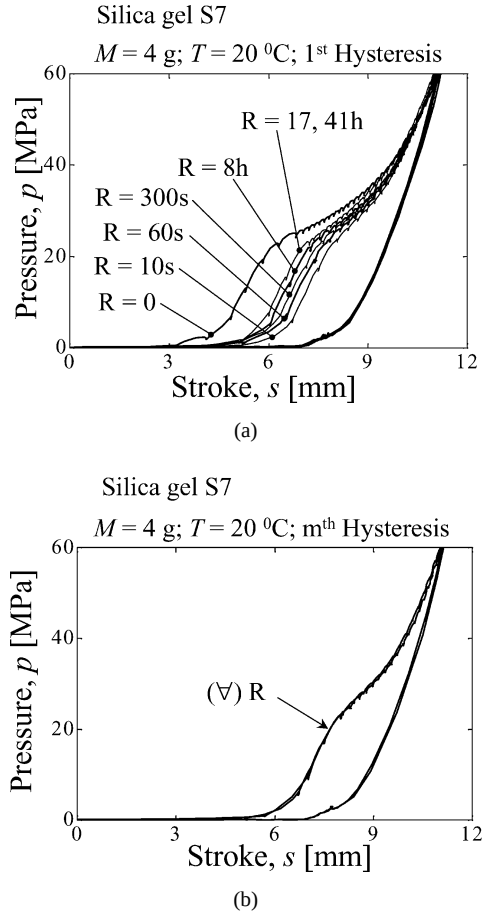


Fig. 16. Influence of the relaxation time on the CD 1st hysteresis (a) and *m*th hysteresis (b).

to partially recover in time, but it never equals the area obtained at the first penetration of the water inside the porous matrix. This feature, never observed at HD, is appropriate for some applications such as seismic dampers and absorbers for the aircraft landing gears. In the case of these dampers, there is always a relaxation period of, at least, several hours in which the CD hysteresis is able to recover. Note also that, after drying in vacuum for 1 h at 80 °C, the colloidal suspension of silica gel S7, collected from the CD test chamber, the largest 1st hysteresis is completely recovered. In other words, with evaporation of the water, which rests captive inside the porous matrix, the cycle fully recovers.

4.8. Mechanism of energy dissipation

In this section, one explains why a hysteresis occurs when the water penetrates and exudes from a hydrophobic porous matrix of silica gel, why the *m*th hysteresis is always smaller than the 1st one, and why the hysteresis partially recovers after a relaxation period. First, one should take into account that every pore represents a distinct geometric space and its shape also has to be taken into consideration [12,16]. Due to the irregularities in the silica gel porous particles, the real shape is known only in a few instances, and models have

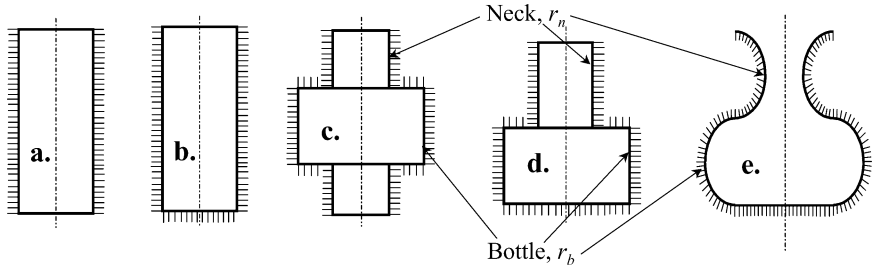


Fig. 17. Models of silica gel pores.

to be employed for an approximation (Fig. 17). The most common model is that of a cylindrical pore, open at one or both ends (Figs. 17a and 17b). Another relates to the so-called "ink-bottle" (neck-bottle) pores, which are described by two radii (Figs. 17c–17e): the radius of the narrow neck r_n and radius of the wide bottle r_b. There have been a number of attempts to explain the hysteresis loop, which occurs in the case of porous materials in the adsorption–desorption process, both for gases and liquids [16]. Particularly for CD, water as the liquid phase penetrates the pores, and in such circumstances, two principal theories of the hysteresis were developed: "ink-bottle" theory, which was accepted by many authors [16,19,22] since it is able to explain the hysteresis revealed both by water and mercury porosimetry; theory of contact angle hysteresis [16,19,54–58], which considers the modification of the contact angle θ during adsorption (advancing) and desorption (receding).

4.8.1. "Ink-bottle" (neck-bottle) theory of hysteresis

One assumes that the neck radius r_n determines the mean compression pressure, and the bottle radius r_b decides the mean relaxation pressure [16]:

$$p_{c,m} = -2\sigma\cos\theta/r_n, \qquad p_{r,m} = -2\sigma\cos\theta/r_b. \tag{22}$$

For pressure ratios $p_{r,m}/p_{c,m} = r_n/r_b$ in the $[0.05; 0.2]$ range (Section 4.3.2), it results that the bottle should be 5–20 times larger than the neck. For instance, in the case of silica gel S6 (Table 2), the neck diameter is about 9 nm, and one expects a bottle diameter of about 45–180 nm. In contrast, no bimodal shape with a second peak in the region of hundreds of nanometers is revealed by the pore size distribution presented in Fig. 4b. Consequently, this theory seems to be unsuitable for the considered silica gels.

4.8.2. Theory of the contact angle hysteresis

This theory [54,56,58] is based on the fact that when the contact angle is dynamically measured (Fig. 18), one can obtain different values, depending on whether it is determined in advancing θ_a (i.e., increasing of the solid–liquid contact area, $d\Omega > 0$) or receding θ_r (i.e., decreasing of the solid–liquid contact area, $d\Omega < 0$). The interval θ_a–θ_r may be of several degrees or several tens of degrees, depending on the surface roughness and chemical inhomogeneities [56]. One defines the equilibrium contact angle as $\theta_0 = (\theta_a + \theta_r)/2$. Contact angle hysteresis explains many phenomena

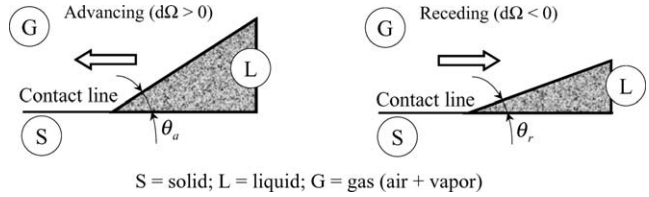


Fig. 18. Contact angle in advancing and receding.

observed in everyday life [58]. For instance, a raindrop attached to a vertical window should flow down under the action of its weight since on a perfect window the capillary force vanishes. On a real window (rough surface), in the upper part of the drop the liquid has a tendency to recede and in the lower part of the drop, the liquid has a tendency to advance. The difference in contact angles creates a capillary force directed upward, which can balance the weight. From a physical standpoint, pinning of the triple contact line on the defects of the solid surface leads to the hysteresis of the contact angle [54–58]. In other words, the interface "finds" the optimal position and angle on the surface, which minimize its free energy [53,54]. Two approaches have been proposed: contact angle hysteresis on a rough surface [55,58] and contact angle hysteresis on a chemical heterogeneous surface [57,58].

4.8.2.1. Contact angle hysteresis on a rough surface. We suppose that chemical inhomogeneities are negligible and the pore surface has a small roughness (Fig. 19). In the simplest model to describe the contact angle hysteresis on a rough surface, one considers a periodic one-dimensional roughness $y = r_0\sin(2\pi x/\lambda)$, the contact line being parallel to the pore [55,58]. Thus, a "composite" structure develops [56], with gas (air and water vapor) bubbles trapped between the liquid and solid (Fig. 19). Contact angle θ occurs as the sum of the equilibrium contact angle θ_0 and the local slope of the solid surface [58]; it reaches its maximum value in advancing ($d\Omega > 0$) and its minimum value in receding ($d\Omega < 0$):

$$\theta_a = \theta_{\max} = \theta_0 + 2\pi r_0/\lambda,$$
$$\theta_r = \theta_{\min} = \theta_0 - 2\pi r_0/\lambda. \tag{23}$$

Dissipated energy due to the contact angle hysteresis on a rough surface E_R occurs as the difference of the excess work

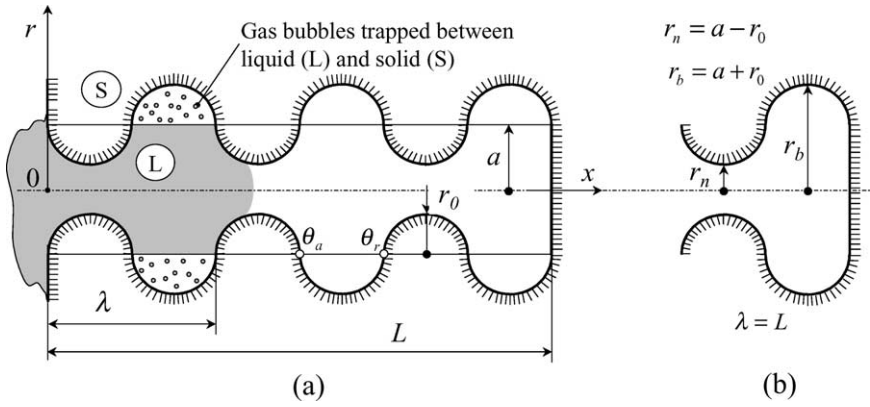


Fig. 19. Model of contact angle hysteresis on the pore rough surface.

done on the system during advancing and receding:

$$E_R = 2MS_{\text{am}}\sigma \sin\theta_0 \sin(2\pi r_0/\lambda). \tag{24}$$

Considering only one sinusoid (Fig. 19b), i.e., $\lambda = L$, we obtain an "ink-bottle" pore structure similar to that presented in Fig. 17e. In other words, the theory of contact angle hysteresis on a rough surface implicitly takes into account for the bottle-neck pore shape, at least when the bottle is not very large. Taking the following data for silica gel S7, $M = 4$ g, $S_{\text{am}} = 250$ m^2/g, $\sigma = 73$ mN/m, $\theta_0 = 114°$, $r_0 = 1$ nm, and $L = 30$ nm, one obtains the dissipated energy due to the surface roughness as $E_R = 28$ J.

4.8.2.2. Contact angle hysteresis on a chemical heterogeneous surface. The solid surface is considered now perfectly smooth but chemically heterogeneous. All defects are assumed as identical and spread at random on the solid surface. The number of defects on the surface unit can be taken as the difference between the theoretical bonding density N_{th} and the real bonding density N of the grafted molecule, i.e., $N_{\text{th}} - N$ (defects/nm^2). Chemical heterogeneity can be considered as a distortion of the contact line, induced by a force per unit length, acting over a distance w of the contact line. Considering rectangular heterogeneities [57], the maximum limit of the heterogeneity as $\sigma(1 - \cos\theta_0)$, and the defect distance as $w = 1.075/N^{0.5}$ [32], the CD dissipated energy due to the chemical inhomogeneities E_C becomes

$$E_C = 0.1MS_{\text{am}}\left(\frac{N_{\text{th}}}{N} - 1\right)\sigma(1 - \cos\theta_0)\ln\frac{LN^{0.5}}{1.075}. \tag{25}$$

Taking data for silica gel S7, $M = 4$ g, $S_{\text{am}} = 250$ m^2/g, $\sigma = 73$ mN/m, $\theta_0 = 114°$, $L = 30$ nm, $N_{\text{th}} = 2.28$ groups/nm^2, and $N = 1.84$ groups/nm^2, one finds the dissipated energy due to the chemical inhomogeneities as $E_C = 9$ J.

Based on the theory of the contact angle hysteresis, one explains the variation of the CD dissipated energy versus relaxation time. The cycle obtained at the first penetration of the water into the porous matrix of silica gel ($R = 0$) is the largest ($E = E_R + E_C = 37$ J, Fig. 20), being determined by the surface roughness and the chemical defects (unmasked

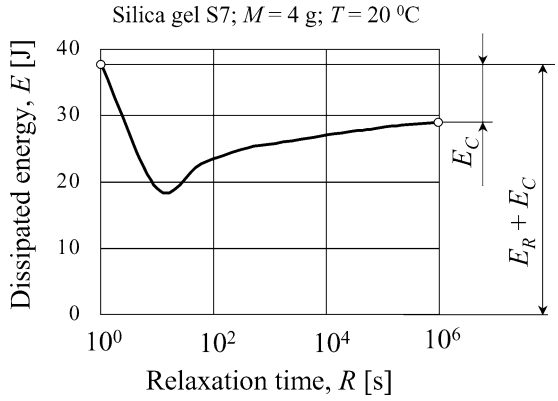


Fig. 20. Influence of the relaxation time on the CD dissipated energy.

OH groups). The difference between the largest and the mth hysteresis is given by the water, which rests captive inside the porous matrix. Water molecules, which develop hydrogen bonds in the regions of unmasked OH groups, can be evacuated only by drying the silica gel matrix. If the relaxation time is long enough, the water trapped on the surface irregularities is slowly pushed out from the silica gel matrix, and the cycle partially recovers. Using Fig. 20, it becomes possible to predict the CD dissipated energy as a function of the loading frequency.

5. Conclusions

1. CD represents a novel and efficient application of nanotechnology in the field of mechanical engineering. CD is a system able to transform the volume work (energy of shock and vibration) into the interfacial work of a solid–liquid–gas boundary. CD dissipated energy can be explained by the theory of the contact angle hysteresis on a rough and chemically heterogeneous surface.
2. In this work, the porous matrix of the colloidal suspension is composed from silica gel modified by linear chains of n-alkylchlorosilanes; water is considered as an associated working fluid. External pressure works

against the Laplace capillary pressure and the pressure of the gas trapped in the porous matrix, which tend to push out the water.

3. Adsorption pressure and the CD dissipated energy varies inversely proportional with the average pore radius. Mean particle diameter, and implicitly the interparticle volume, has no influence on the CD hysteresis.
4. The silica gel surface requires hydrophobic modification to obtain a large and reproducible cycle. Hysteresis shape depends on the bonding density and the length of the grafted molecule.
   - 4.1. From a thermal standpoint, the C1 coating is more stable than the C18 one. From the pressurization point of view, the C18 coating is more stable than the C1 one.
   - 4.2. The slope of the central zone of the curve of dimensionless energy versus dimensionless pressure is related to the length of the grafted molecule.
   - 4.3. CD with irreversible, large 1st hysteresis can be used as a shock absorber. CD with reversible, large 1st hysteresis can be employed for vibration reduction.
5. CD maximum efficiency is reached at the optimum loading pressure and optimum quantity of water, which equals the pore volume of the silica gel matrix.
6. With mixing of silica gels with different levels of hydrophobicity, length of the grafted molecule, and/or particle architecture, the shape of the hysteresis can be controlled.
7. For piston speeds smaller than a critical velocity, the CD cycle can be considered as isothermal. Heat due to the viscous effects is negligible since the water flow into the mesopores space occurs as creeping and laminar with slippage at the solid walls, which approaches a potential flow. Shape of the CD hysteresis is relatively insensitive to the temperature modifications since the water surface tension has slow variation with temperature. In contrast, the HD dissipated energy is considerably affected by the temperature changes since the mineral oil viscosity sharply varies against temperature.
8. The CD cycle has the ability to partially recover in time, but it never equals the area obtained at the first penetration of the water inside the porous matrix. This feature, never observed at HD, is useful in some applications, such as seismic dampers and absorbers for the aircraft landing gears.
9. The CD maximum efficiency (54–97%) is higher than the HD maximum efficiency (30–40%).
10. Our results agree with the previously published experimental data.

Acknowledgments

The authors would like to acknowledge support by the Oiles Corporation, Tokyo. We would like to thank Dr. Kazuhiko Yaguchi at Fuji Silysia Chemical Ltd., Nagoya, for his help in providing hydrophobic silica gel and available data concerning the particles and pore distributions.

Appendix A. Nomenclature

a ($2a$)	Pore radius (diameter) (m)
A	Molecule or liquid cluster
AB	Clathrate
b ($2b$)	Microparticle radius (diameter) (m)
B	Molecule or cavity of a solid microparticle
c	Compressibility (Pa^{-1})
d	Diameter of the piston rod (m)
D	Piston diameter (m)
D^*	Collision diameter (m)
D_{ha}	Diameter of the hydraulic amplifier (m)
DTA	Differential thermal analysis (μV)
E	Dissipated energy (J)
E_a	Absorbed energy (J)
E_C	Dissipated energy due to the chemical inhomogeneities (J)
E_R	Dissipated energy due to the surface roughness (J)
F	Force (N)
h	Thickness of the bonded hydrophobic layer (m)
$k_{1,2,3,4}$	Constants defined in Eq. (3) ($Pa\,s\,K^{\gamma}$, K^{-1}, K^{-2}, K^{-3})
Kn	Knudsen number, L_p/L
L	Mean length of the pore (m)
$\bar{L}$	Dimensionless mean length of the pore, L/a
L_p	Molecular free path (m)
m	Number of the hysteresis ($m \geqslant 2$)
M	Mass of silica gel (g)
M_0	Added mass of fluid (kg)
M_m	Molar mass of a modifier (g/mol)
n	Number of carbon atoms in the C_nH_{2n+1} linear chain
n_c	Number of carbon atoms in the grafted molecule
N	Bonding density (group/nm^2)
$N_{1,2,3}$	Bonding density limits (group/nm^2)
N_{th}	Theoretical bonding density (group/nm^2)
p	Pressure (Pa)
$\bar{p}$	Dimensionless pressure, p/p_0
p_0	Atmospheric pressure (Pa)
p_c	Compression pressure (Pa)
$p_{c,m}$	Mean compression pressure (Pa)
p_g	Gas pressure (Pa)
p_r	Relaxation pressure (Pa)
$p_{r,m}$	Mean relaxation pressure (Pa)
P_c	Carbon percentage (by weight) in the modified silica gel (%)
q	Flow rate delivered by the pump (m^3/s)
Q	Heat (J)
r	Radial coordinate (m)
r_0	Amplitude of the periodical one-dimensional roughness (m)

r_b	Bottle radius (m)
r_n	Neck radius (m)
R	Relaxation time (s)
$R(x, u_m)$	Flow resistance (N)
Re	Reynolds number, $2\rho u_m a/\mu$
s	Piston stroke (m)
S	Specific surface (m^2/g); Entropy (J/K)
S_p	Surface of the open ends of the pores, $V_{p,\mathrm{am}}/L$ (m^2/g)
t	Time (s)
$\bar{t}$	Dimensionless time, t/t_c
t_c	Compression time (s)
T	Temperature (°C, K)
T_0	Reference temperature (K)
T_c	Critical temperature (K)
TG	Weight loss (mg)
u	Velocity in the x direction (m/s)
u_m	Mean velocity in the x direction (m/s)
u_s	Slip velocity (m/s)
U	Internal energy (J)
v	Piston velocity (m/s)
V	Volume (m^3)
V_p	Pore volume (ml/g)
V_s	Silica gel volume (m^3)
V_w	Water volume (m^3)
w	Defect distance (m)
W	Work (J)
W_c	Compression work (J)
x	Axial coordinate (m)
$\bar{x}$	Dimensionless axial coordinate, x/a
y	Periodic one-dimensional roughness (m)
ΔT	Temperature variation (°C, K)
ΔU	Internal energy variation (J)
Φ	Dissipation rate (J/m^3)
γ	Constant defined in Eq. (3)
Γ	Dimensionless parameter, $\rho_0 a^2/(p_0 t_c^2)$
η	Damper efficiency, $100E/E_a$ (%)
η_HD	HD maximum efficiency, $100[1-(d/D)^2]$ (%)
λ	Period of the one-dimensional roughness (m)
μ	Dynamic viscosity (Pa s)
μ_0	Dynamic viscosity at the atmospheric pressure (Pa s)
θ	Contact angle (deg)
θ_0	Equilibrium contact angle, $(\theta_a+\theta_r)/2$ (deg)
θ_a	Advancing contact angle (deg)
θ_r	Receding contact angle (deg)
ρ	Density (kg/m^3)
ρ_0	Density at atmospheric pressure (kg/m^3)
σ	Surface tension (N/m)
$\bar{\sigma}$	Dimensionless surface tension, $\sigma/(ap_0)$
σ_c	Constant surface tension (N/m)
Σ	Interface
Ω	Interface area (m^2)

Subscripts

am (bm)	After (before) modification
max	Maximum
mean	Mean
min	Minimum
T	Constant temperature
V	Constant volume

Superscripts

no-slip	Refer to the no-slip flow
slip	Refer to the slip flow

Abbreviations

AE (BE)	After (before) experiment in the CD test chamber
CD	Colloidal damper
C1 (C18)	$-Si(CH_3)_2C_nH_{2n+1}$ linear chain of alkylsilane for $n=1$ ($n=18$)
DTA-TG	Differential thermal analysis
G	Gas
HD	Hydraulic damper
L	Liquid
N_2	Nitrogen adsorption (Cranston–Inkley method)
S	Solid
S1–S11	Silica gels 1–11

References

[1] N.P. Chironis, Spring Design and Application, McGraw–Hill, New York, 1961.
[2] C.M. Harris, C.E. Crede, Shock and Vibration Handbook, McGraw–Hill, New York, 1968.
[3] C.V. Suciu, O. Bonneau, D. Brun-Picard, J. Frene, M.D. Pascovici, ASME J. Tribol. 122 (2000) 211.
[4] C.V. Suciu, T. Iwatsubo, M.D. Pascovici, ASME J. Tribol. 124 (2002) 480, doi: 10.1115/1.1454101.
[5] R. De la Taille, Sci. Vie 939 (1995).
[6] V.A. Eroshenko, Patent 94/14856 (1994) 1.
[7] V.A. Eroshenko, Patent WO 01/55616 A1 (2001) 1.
[8] V.A. Eroshenko, R.C. Regis, M. Soulard, J. Patarin, J. Am. Chem. Soc. 123 (2001) 8129.
[9] C.V. Suciu, T. Iwatsubo, S. Deki, in: JSME Damping Symposium II, Tokyo, Japan: Proceedings, 2002, p. 282.
[10] R.K. Iler, The Chemistry of Silica—Solubility, Polymerization, Colloid and Surface Properties, and Biochemistry, Wiley, New York, 1979.
[11] L.R. Snyder, J.J. Kirkland, Introduction to Modern Liquid Chromatography, 2nd ed., Wiley, New York, 1979.
[12] K.K. Unger, Porous Silica—Its Properties and Use as Support in Column Liquid Chromatography, Elsevier, Amsterdam, 1988.
[13] L.A. Belyakova, A.M. Varvarin, Colloids Surf. A 154 (1999) 3.
[14] A.Y. Fadeev, V.A. Eroshenko, J. Colloid Interface Sci. 187 (1997) 275.
[15] R. Defay, I. Prigogine, A. Bellemans, D.H. Everett, Surface Tension and Adsorption, Longmans, London, 1966.
[16] S.J. Gregg, K.S.W. Sing, Adsorption, Surface Area and Porosity, Academic Press, San Diego, 1982.
[17] R.I. Masel, Principles of Adsorption and Reaction on Solid Surfaces, Wiley, New York, 1996.

[18] D.M. Ruthven, Principles of Adsorption and Adsorption Processes, Wiley, New York, 1984.
[19] V.A. Eroshenko, A.Y. Fadeev, Colloid J. 57 (1995) 4.
[20] V.A. Eroshenko, A.Y. Fadeev, Russ. J. Phys. Chem. 70 (1996) 8.
[21] V.A. Eroshenko, in: 5th World Congress on Joints, Bearings and Seismic Systems for Concrete Structures, Rome, Italy, 2001.
[22] T. Iwatsubo, C.V. Suciu, S. Deki, in: Asia-Pacific Vibration Conference, Hangzhou, China: Proceedings, Vol. 2, 2001, p. 407.
[23] V.A. Eroshenko, Colloid J. 49 (1987) 5.
[24] V.A. Eroshenko, Mendeleev Chem. J. 39 (1995) 2.
[25] T. Reis, Introduction a la Chimie-Physique des Surfaces, Dunod, Paris, 1952.
[26] M.D. Hersey, Theory and Research in Lubrication, Wiley, New York, 1966.
[27] B.O. Jacobson, Rheology and Elastohydrodynamic Lubrication, in: Tribology Series, Vol. 19, Elsevier, Amsterdam, 1991.
[28] C.H. Cho, J. Urquidi, G.W. Robinson, J. Chem. Phys. 111 (1999) 22.
[29] H.A. Barnes, J.F. Hutton, K. Walters, An Introduction to Rheology, Elsevier, Amsterdam, 1989.
[30] P.W. Bridgman, The Physics of High Pressure, Bell, London, 1958.
[31] J. Clifford, Water a Comprehensive Treatise—Properties of Water in Capillaries and Thin Films, Pergamon, New York, 1993.
[32] A.Y. Fadeev, S.M. Staroverov, J. Chromatogr. 447 (1988) 103.
[33] A.Y. Fadeev, S.M. Staroverov, J. Chromatogr. 465 (1989) 233.
[34] S.M. Staroverov, A.Y. Fadeev, J. Chromatogr. 544 (1991) 77.
[35] H. Naono, M. Hakuman, T. Tanaka, N. Tamura, K. Nakai, J. Colloid Interface Sci. 225 (2000) 411, doi: 10.1006/jcis.2000.6777.
[36] T. Takei, A. Yamazaki, T. Watanabe, M. Chikazawa, J. Colloid Interface Sci. 188 (1997) 409.
[37] R.G. Avery, J.D.F. Ramsay, J. Colloid Interface Sci. 42 (1973) 597.
[38] W. Huang, R.S. Bhullar, Y.C. Fung, ASME J. Biomech. Eng. 123 (2001).
[39] G.K. Batchelor, An Introduction to Fluid Dynamics, Cambridge University Press, Cambridge, 1967.
[40] F.M. White, Viscous Fluid Flow, McGraw–Hill, New York, 1974.
[41] D. Frenkel, B. Smit, Understanding Molecular Simulation—From Algorithms to Applications, Academic Press, New York, 1996.
[42] J. Happel, H. Brenner, Low Reynolds Number Hydrodynamics with Special Applications to Particulate Media, Nijhoff, Dordrecht, 1986.
[43] W.E. Langlois, Slow Viscous Flow, Macmillan, New York, 1964.
[44] T.M. Patzek, D.B. Silint, J. Colloid Interface Sci. 236 (1973) 295.
[45] O.I. Vinogradova, Int. J. Miner. Process. (1999) 56.
[46] E. Schnell, J. Appl. Phys. 27 (1956) 10.
[47] N.V. Churaev, D.V. Sobolev, A.N. Somov, J. Colloid Interface Sci. 97 (1984) 574.
[48] H. Wang, in: International Tribology Conference, Nagasaki, Japan: Proceedings, 2000, 1F4-1.
[49] S.C. McGrother, K.E. Gubbins, J. Mol. Phys. 97 (1999) 8.
[50] E. Sakir, E. Guneyler, Physica E 8 (2000).
[51] N.S. Isaacs, Liquid Phase High Pressure Chemistry, Wiley, New York, 1981.
[52] H. Kuhn, H.D. Forsterling, Principles of Physical Chemistry, Wiley, New York, 1999.
[53] J. Lyklema, Fundamentals of Interface and Colloid Science, Vols. 1 and 2, Academic Press, London, 1991/1995.
[54] S.A. Safran, Statistical Thermodynamics of Surfaces, Interfaces and Membranes, Addison–Wesley, New York, 1994.
[55] R.G. Cox, J. Fluid Mech. 131 (1983) 1.
[56] P.G. Gennes, Rev. Mod. Phys. 57 (3) (1985) 827.
[57] J.F. Joanny, P.G. Gennes, J. Chem. Phys. 81 (1984) 1.
[58] L. Leger, J.F. Joanny, Rep. Prog. Phys. 55 (1992) 431.
[59] D.R. Lide, CRC Handbook of Chemistry and Physics, 80th ed., CRC Press, Boca Raton, FL, 1999.
[60] G.S. Kell, J. Chem. Eng. Data 20 (1975) 1.